Bioinspiration & Biomimetics



RECEIVED

26 July 2018 REVISED

24 October 2018

ACCEPTED FOR PUBLICATION 15 November 2018

PUBLISHED

18 December 2018

PAPER

Analog control with two Artificial Axons

Hector G Vasquez and Giovanni Zocchi

Department of Physics and Astronomy, University of California, Los Angeles, CA, United States of America

E-mail: zocchi@physics.ucla.edu

Keywords: complex systems, biomimetics, action potentials, cybernetics

Supplementary material for this article is available online

Abstract

The artificial axon is a recently introduced synthetic assembly of supported lipid bilayers and voltage gated ion channels, displaying the basic electrophysiology of nerve cells. Here we demonstrate the use of two artificial axons as control elements to achieve a simple task. Namely, we steer a remote control car towards a light source, using the sensory input dependent firing rate of the axons as the control signal for turning left or right. We present the result in the form of the analysis of a movie of the car approaching the light source. In general terms, with this work we pursue a constructivist approach to exploring the nexus between machine language at the nerve cell level and behavior.

Introduction

Action potentials form the machine language of the nervous system. While the mechanisms and characteristics of action potentials have been known for over half a century, these most interesting excitations have not been produced in vitro, in a synthetic biology setting, until very recently [1]. The artificial axon (AA) [1, 2] is an excitable node which supports action potentials, that is, voltage spikes produced by the same ionic mechanism as action potentials in neurons. Our aim is to develop it into a platform for synthetic biology constructions which echo neuronal systems. Since the AA works, as far as electrical excitability, through the same physical mechanism as the real neuron, it can be endowed with some of the same capabilities, and also suffers from similar constraints. Learning to build useful networks within these constraints is a viable engineering approach to understanding brain function. Existing constructive approaches are computational [3], electronic [4, 5], or based on real neurons, directing their pattern of connection [6–11], and re-programming stem cells in 3D cultures [12]. Especially the first two are much more advanced than what we show here; they also have a longer history, and, crucially, they are based on electronics. Specifically, neuromorphic chips (NMCs) are currently competitive with traditional von Neumann architecture neural networks in solving complex problems in pattern recognition [13]. However, NMCs are simulators of spiking nerves, based on a fundamentally different microscopic process, namely electronics. Although the higher level architecture may be designed similar to a real network of neurons, the microscopics is different. Cultured neurons have been used by the Moses group to construct logic functions such as AND, also demonstrating a remarkable reliability achieved through a redundancy of connections [10]. Potter and Marom have reported using neurons on microelectrode arrays (MEAs) in control systems to move robots [14, 15], yielding interesting design directions. For example, a control system with neurons on an MEA has moved an airplane in a flight simulator [16]. Our approach is an attempt to simplify the patterned neuron paradigm, by introducing a simpler, synthetic 'neuron'. In contrast to NMCs, AAs are to be based on the same microscopic process as real neurons, namely ionics. This is, we believe, an incisive experimental approach to study how the microscopics of neurons may generate complex macroscopic responses, patterns, and behaviors. The latter program partakes of the underlying thread of condensed matter physics, and our approach is informed by that discipline.

Coming back to NMCs, interest in the field is both scientific and practical, the latter because NMCs based AI may enjoy possibly orders of magnitude better energy consumption characteristics compared to von Neumann architecture AI. AA chips could in principle enjoy similar architectural advantages, plus additional power saving benefits due to the fact that ionics circuitry works at \sim 100 mV versus the \sim 1 V of electronic circuitry [1]. However, it should be mentioned that where power density is the sole criterion, notwithstanding, for example, portability, there are low temperature devices which can fare much better [17]. Our objective with the AA in the near future is to develop a breadboard or 'tool kit' with which to construct task performing networks which are based on the same microscopics as neurons, and therefore are 'possible brains'. At the moment, even one AA is sufficiently delicate, and complicated to make, that we thought it would be useful to give a demonstration of an actual task performing device based on AAs, even though we can only make very simple ones at present. Namely, we use a system of two AAs to steer a remote control toy car towards a light source.

First, we briefly describe the AA, which was introduced previously [1, 2], and give an overview of the present system. In the next section, we describe the results: they consist of a demo in the form of a movie, with accompanying analysis. In materials and methods we describe in detail the EE aspects, in order to report exactly what we do with the AAs and the electronic circuitry. We conclude with a brief discussion of relevance and scope.

The present AA is an excitable 100 μm size 'node' consisting of a supported phospholipid bilayer with \sim 100 voltage gated potassium channels (KvAP) embedded and oriented. A concentration gradient of potassium ions is maintained across the bilayer by means of reservoires; typically $[K^+]_{in} \approx 30$ mM for the 'inside' of the axon and $[K^+]_{out} \approx 150$ mM for the 'outside'. In the following, all potentials represent the potential difference between the inside and outside of the axon: $V = V_{in} - V_{out}$. The aforementioned ionic gradient results in an equilibrium (Nernst) potential

$$V_N = \frac{kT}{|e|} \ln \frac{[K^+]_{out}}{[K^+]_{in}} \approx +40 \text{ mV}.$$
 (1)

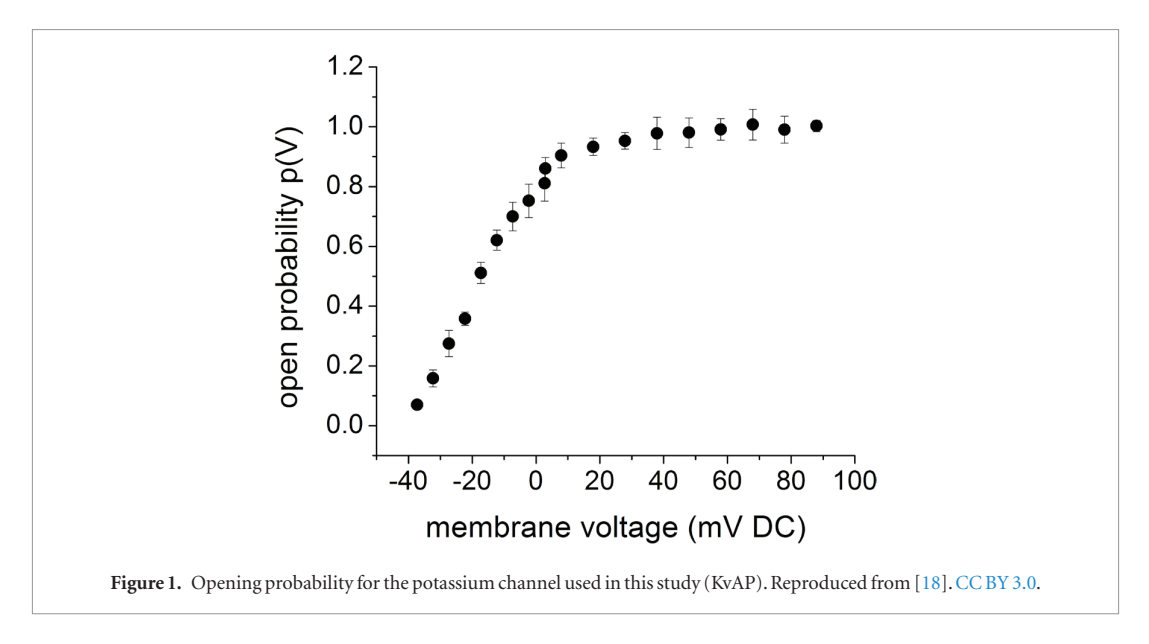
Here, $kT \approx 25$ meV is the thermal energy at room temperature and e the electronic charge. In the real neuron, there is in addition an opposite gradient of sodium ions across the membrane, which results in a 'resting potential' V_r intermediate between the Nernst potentials of the K^+ and Na^+ ions, and corresponding voltage gated sodium channels. In the AA, that role is played by the current limited voltage clamp (CLVC) [2], which keeps the AA voltage out of equilibrium, typically at a 'resting potential' $V_r \approx -120$ mV. The response curve of the KvAP channels (figure 1) shows that they are closed at $V = V_r = -120$ mV, but if a stimulus brings the voltage above $V \sim -20$ mV the channels open, the chemical potential driven channel current overwhelms the CLVC current, and the AA 'fires'. The subsequent inactivation of the KvAP channels, which stochastically enter a third, closed, state, allows the CLVC to pull the membrane potential back to the resting value. In figure 2 we show a train of two action potentials in an artificial axon. The input stimulus is a constant current (\sim 128 pA), delivered with a current clamp. The membrane potential V_m is measured through a separate electrode, and

corresponds to the ordinate scale on the left in the figure. The dotted trace represents the command voltage V_c to the CLVC, and corresponds to the ordinate scale on the right. Instead of simply keeping V_c constant at ~ -364 mV, which would maintain, in this case, a resting potential $V_m \approx -120$ mV, the protocol for V_c is that when the axon 'fires', V_c is lowered to -636 mV for a fixed time (= 1 s), then returns to -364 mV. This maneuver is necessary but incidental to the particular inactivation dynamics of the ion channel we are using (the KvAP). Namely, after a firing we must pull the membrane potential V_m down to about -150 mV in order that the channels re-activate fast enough to be ready for the next firing.

Note the slow channel dynamics in comparison to channels of animal neurons: ∼1 Hz firing rates in the AA, ∼1 kHz in animal cells. The KvAP is a bacterial channel, from Aeropyrum pernix, a thermophile discovered in deep-sea vents in the Pacific Ocean, where the temperature is \sim 90 °C. On the other hand, all experiments with the AA are performed at room temperature. In our conditions, the characteristic time scale for opening the channels is $\tau(c \to o) \sim 25$ ms, the time scale for inactivation is $\tau(o \rightarrow i) \sim 400$ ms, and the time scale for re-activation is very much membrane potential dependent: at 0 mV it is $\tau(i \rightarrow c; 0 \text{ mV}) \sim 100 \text{ s}; \text{ at}$ —150 mV it is $\tau(i \rightarrow c; -150 \text{ mV}) \sim 1.4 \text{ s}$ (c: closed; o: open; i: inactive). These are reported, for our conditions, in the supplementary material section of [1] (stacks. iop.org/BB/14/016017/mmedia). Our slow firing rate results from the combination of these time scales, plus the need to keep the resting potential quite low $(V_r \sim -150 \,\mathrm{mV})$ in the experiments) so that the recovery rate from inactivation is not too slow. The overall width of the action potential in our system is then mostly the result of the following. For the rising edge, the time it takes to charge the membrane capacitance from a very negative V_r to the threshold for firing $(\sim -20 \,\mathrm{mV})$. For the falling edge, the slow rate of inactivation.

With all these drawbacks, why do we use the KvAP? Because it is robust and well characterized [19–22], the protocols for expression and purification are well documented [23–25], and we have experience with it in the Lab [2, 26]. However, in the future we aim to replace the KvAP with a faster potassium channel, and to introduce a second channel to replace the CLVC.

We have previously documented some basic electrophysiology with this system, such as integrate-and-fire dynamics [1]. For our present purpose, we use two AAs as a control module to steer a toy car towards a light source. Figure 3 shows a diagram of the system. The AAs sit on an optical table in the lab; communication with the car is by radio waves. The remote control car is modified with two sets of photodiodes ('eyes') accepting light from the right (R) and left (L) side of the car, respectively, and corresponding voltage-to-frequency converters (VFCs) and transmitters.



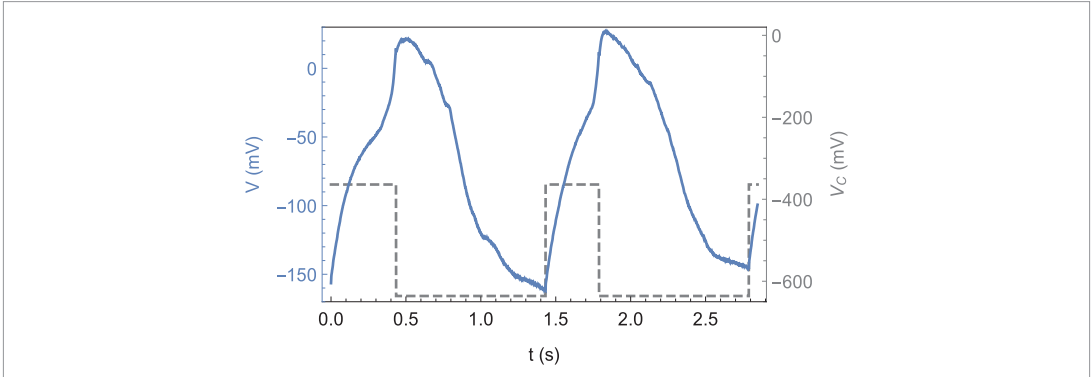
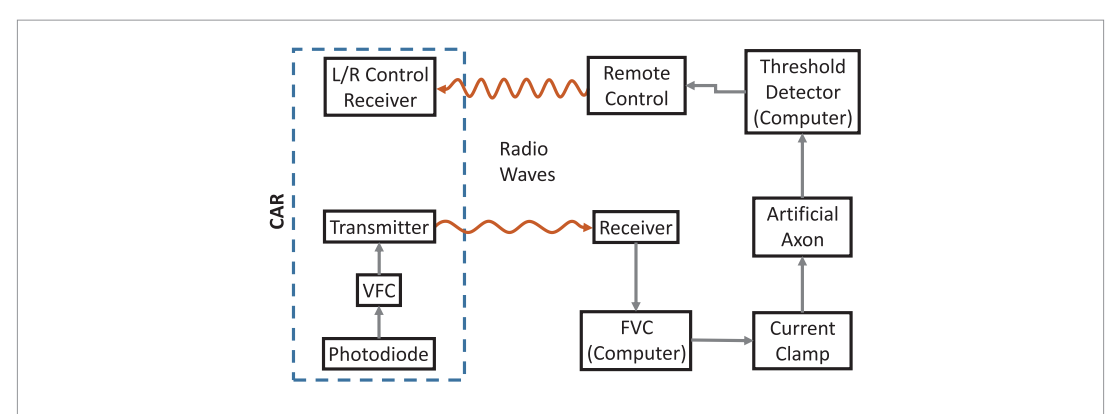


Figure 2. Action potentials in the AA, elicited by a constant current input. Plotted is the measured membrane potential $(V_m$: left scale). The dotted trace shows the protocol of the CLVC $(V_c$: right scale). The downward step in V_c is triggered by V_m crossing 10 mV; see text for explanations.



 $\textbf{Figure 3.} \ \ System \ block \ diagram. \ The \ complete \ system \ consists \ of \ two \ such \ circuits, one \ for \ the \ right (R) \ photodiodes \ and \ AA \ and \ one \ for \ the \ left (L) \ components. \ VFC: \ voltage \ to \ frequency \ converter; \ FVC: \ frequency \ to \ voltage \ converter.$

Following for example the signal from the R photodiode, its voltage output is converted to frequency (in the kHz range) by the VFC and transmitted; this signal is received by a receiver on the optical table, converted to voltage by another VFC, and used as the input to a current clamp, or 'synapse', which injects a proportional current (in the tens of pA range) into the right (R)

axon. Action potentials in the AA trigger a threshold detector which inputs into the remote control module of the car the signal to turn the wheels to the right. We use the actual remote control of the toy car, and so the same receiver and right/left control built into the car. A similar but independent pathway conditions the signal from the left photodiode set. In summary, this



Figure 4. Still of the room of the demo, seen from the ceiling. The car and light source are at diametrically opposite corners. Visible on the right is the optical table with the artificial axons and the electronics, as well as one of the the authors (H.G.V.).

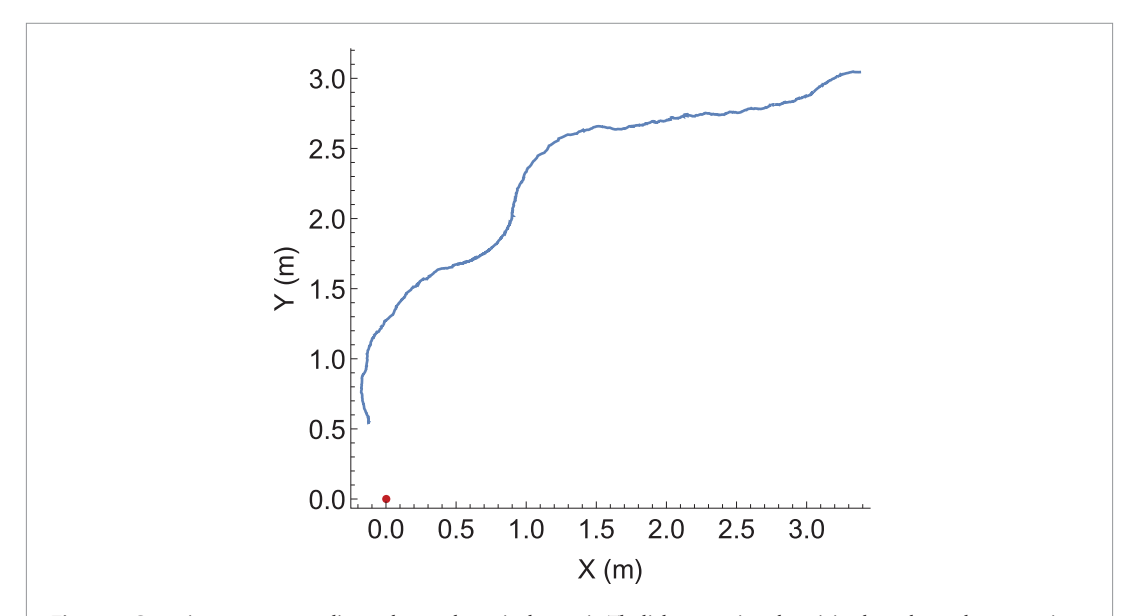


Figure 5. Car trajectory corresponding to the run shown in the movie. The light source is at the origin; the scales on the axes are in m, and the car starts at (x, y) = (3.4, 3.0).

system realizes a very simple analogue control protocol: each time the R axon spikes, the wheels of the car are turned to the right and stay there until the next signal comes in, and similarly for the L axon, which turns the wheels to the left. Action potentials in the R/L axon are induced by the light intensity falling onto the R/L photodiode set. So while all the peripheral systems are, at the moment, electronic, the 'decision making algorithm' is implemented by ionics.

There is no interaction between the two AAs in this realization, and the only property of the AA which we really exploit is the 'integrate-and-fire' dynamics. The system has a degree of stochasticity (due to the relatively small number of ion channels in the axons), lots of noise which is not only thermal in origin, makes many mistakes, has many defects, and ends up looking 'biological' (see movie in supplementary data files).

Results

The main result we present is a demonstration of the system in the form of the accompanying movie (see ancillary files), which we now describe. The car moves in a (previously decluttered) laboratory room of about 5×5 m²; in the movie, the light source is in the SW corner of the screen, and the car starts at the NE corner, facing W. The other bright spots on the screen are reflections of the light source from objects at the periphery of the room. Figure 4 is a picture of the room seen from the ceiling.

In the movie, watch the front wheels of the car repeatedly switch between L and R, and the overall progress. We had to slow down the speed of the car to match it to our rather slow axons, so we adopted short, regular spurts of forward motion. The actual average speed of the car is however not constant, as you see in the movie, because at times the tires slip on the polished floor. From an engineering standpoint, we may view this circumstance as simply one of many 'defects' or sources of noise in the system. There are many such sources of randomness, from the microscopic scale of the individual ion channels in the AA to the macroscopic scale of the tires. As a result, the trajectory of the car, the 'behavior', is not deterministic (starting from

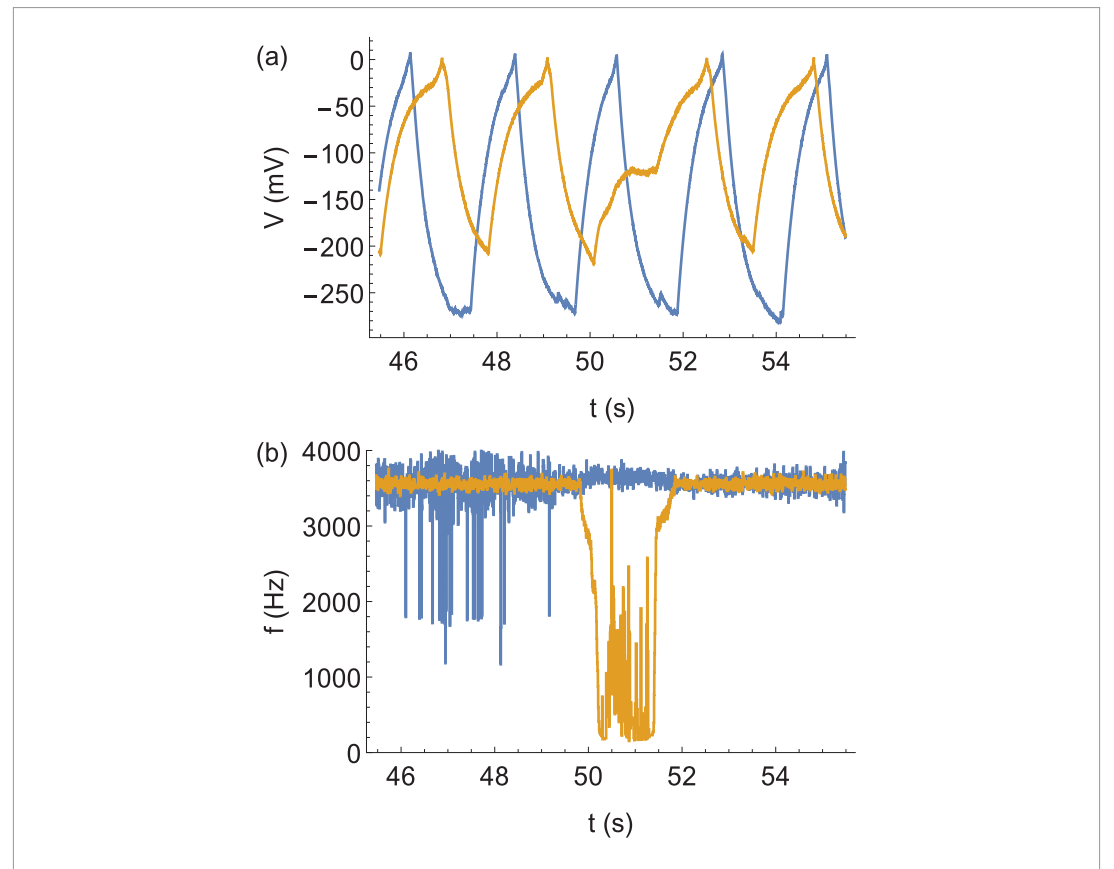


Figure 6. (a) Membrane potential in the left artificial axon (blue trace) and the right AA (yellow trace) for part of the run shown in the movie. (b) The signal at the output of the voltage to frequency converter (VFC), for the R and L circuits, and the same time interval as in (a). The currents injected by the synapses into the respective AAs are proportional to these signals.

identical initial conditions, different realizations of the car's trajectory will be different); however, the car does find the light source in the end. Figure 5 shows the trajectory corresponding to the movie.

Let us now describe the very simple 'machine language' with which the system operates. Figure 6(a) shows action potentials in the two AAs over a time of 10 s; the blue trace is the membrane potential of the left AA, the yellow trace is the right AA. The response of the car is that when the blue trace crosses 4.5 mV from below, the wheels turn left and stay there until further notice; similarly, when the yellow trace crosses 0 mV, the wheels turn right and stay there. What decides, then, whether overall the car is turning L or R is the relative phase of the spikes in the two AAs. In the example shown, for 45 < t < 50.5 s the car is, overall, turning R because the time interval between a yellow and the next blue zero crossing is larger than the time between a blue and the next yellow. On the other hand, for 50.6 < t < 56 s the car is overall turning L; this is a consequence of the R photodiodes seeing less light for 50 < t < 52 s (figure 6(b)), which causes a delay in the yellow spikes, changing the phase relation between blue and yellow spikes. Even with identical stimuli (input currents from the 'synapses'), the firing rates of the two AAs are not the same (due to physical differences between the AAs, for instance, different number of ion channels, different leak currents, etc). This

circumstance introduces 'phase noise', yet another source of (non-thermal) stochasticity which however does not prevent the overall working of the system. That is, the two AAs do not need to be perfectly tuned as far as firing rates.

Figure 6(b) shows, for the same run as in part (a), the frequency coming out of the voltage to frequency converter, for the L (blue) and R (yellow) circuit. The current injected by the corresponding 'synapse' into the L/R axon is proportional to this frequency. While the firing rates of the two AAs do not need to be perfectly tuned, if, for equal light, one firing rate is larger than the other, this introduces a bias in the approach to the light source. In the realization shown in figure 5, the right AA had a faster firing rate, and a right turn bias is visible in the trajectory. We come back to the question of how much difference in firing rates can be tolerated in the discussion.

In figure 7 we report the whole time series for the two AAs corresponding to the run of the movie, and in figure 8 two different representations, among the many possible ones, of the 'behavior' of the car.

Materials and methods

In this section, we describe in detail the EE aspetcs of the demo, and summarize the construction and operation of the AA; the latter has been described before [1,2].

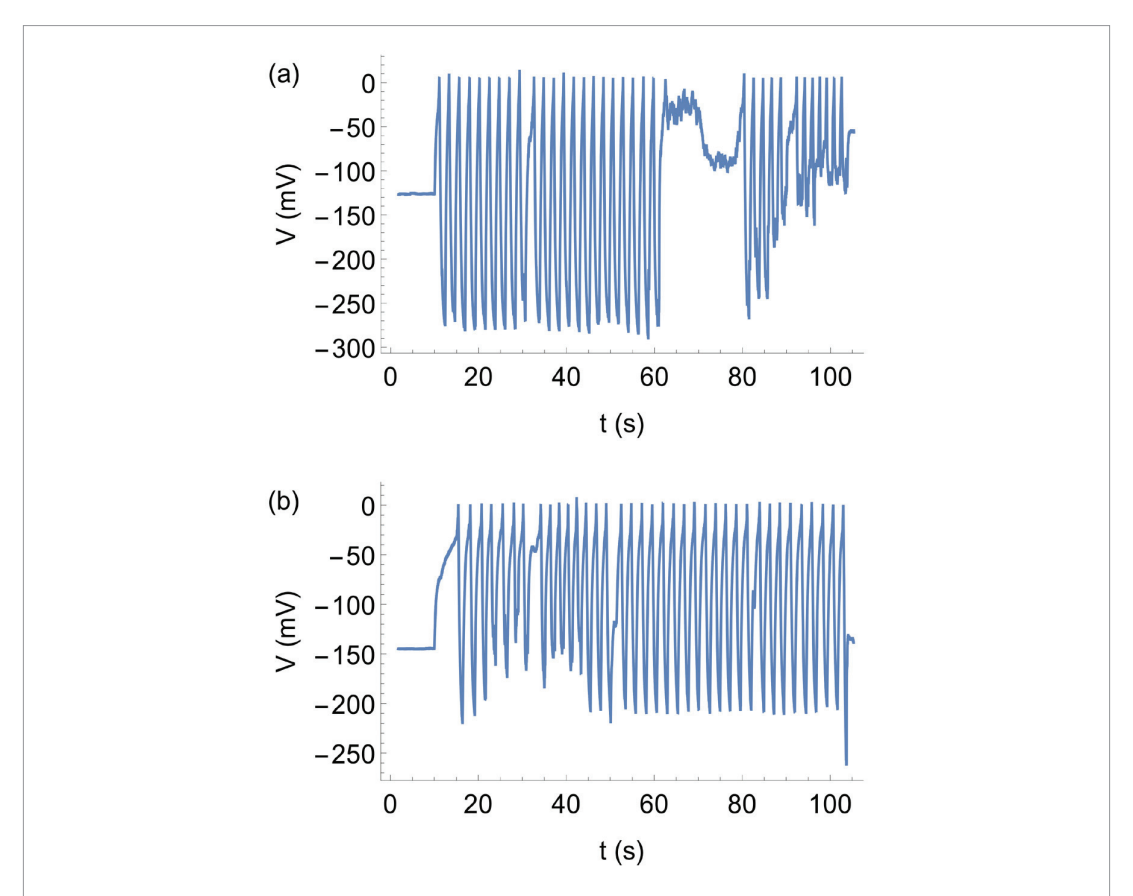
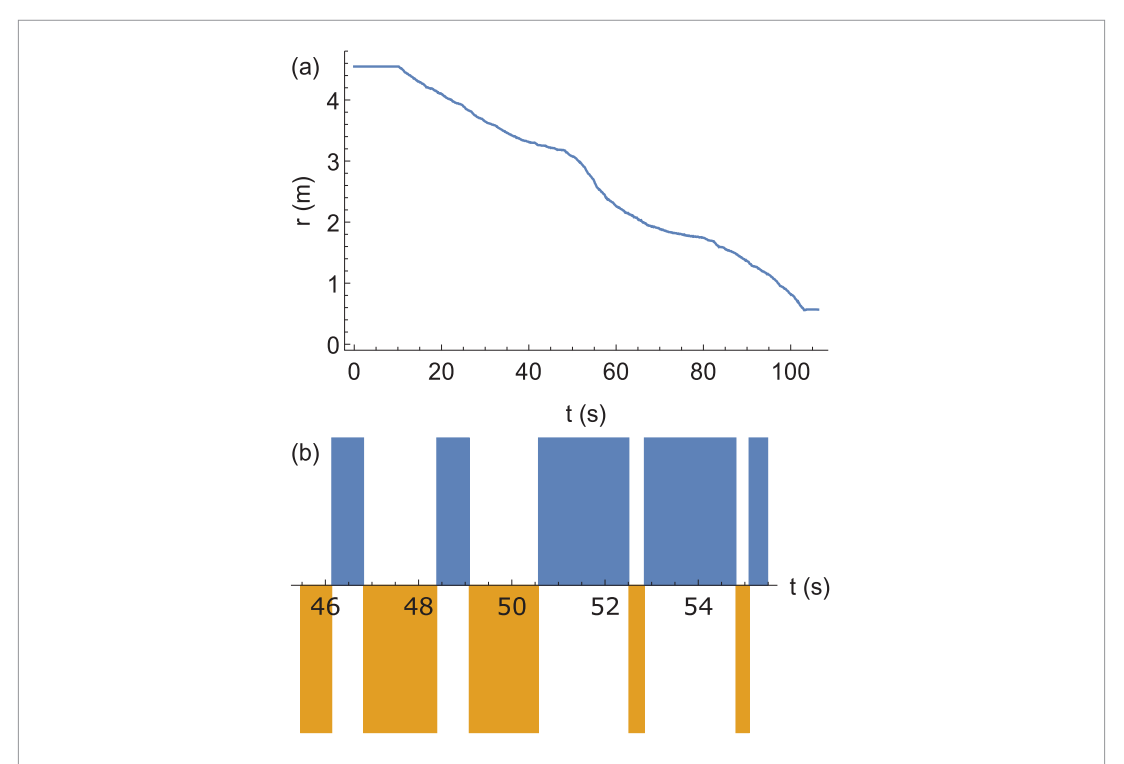
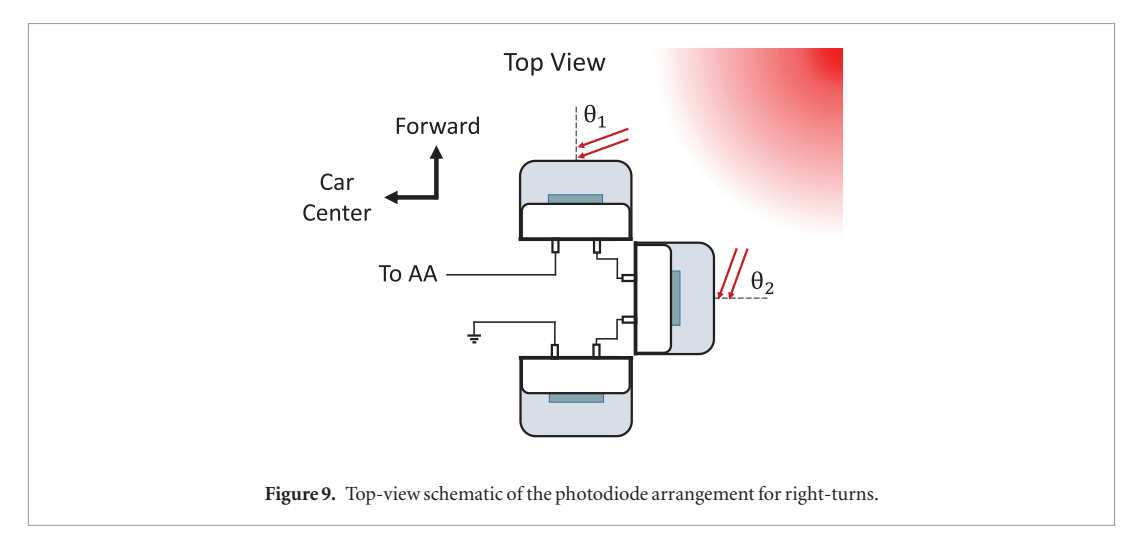


Figure 7. Whole time series of action potentials corresponding to the run of the movie. Time t = 0 s corresponds to the start of the video. The data recording begins 1.75 s later. (a) Left axon; (b) right axon.



 $\textbf{Figure 8.} \ \ (a) \ \, \text{Distance from the target versus time, calculated for the trajectory of figure 5;} \ (b) \ \, \text{time series showing intervals when the car is turning left } \ \, (+1) \ \, \text{and right } (-1). \ \, \text{This plot corresponds to the spike trains of figure 6.}$



Molecular biology

The KvAP gene in vector pQE60 is expressed in *Escherichia coli* strain XL1-Blue competent cells (Aligent) and reconstituted in DPhPC vesicles. In the experiments, vesicles are fused to the lipid bilayer from one side, resulting in oriented channels. The channels are oriented in the vesicles with the extracellular side of the channel oriented toward the inside of the vesicle. Presumably, this is due to the curvature of the vesicle. We address channel orientation in previous work with the same system. Protein expression, purification, reconstitution protocols and channel orientation are discussed and described at length in previous publications [1, 2, 18, 26].

The 'eyes' of the car

For each eye, three Burr-Brown OPT 301 photodiodes are positioned at 90 degrees relative to each other. This arrangement is shown in figure 9 for right eye. One photodiode faces the direction of forward motion, another is oriented 180 degrees relative to the first in the backward direction, and the third is perpendicular to the other two, facing outward. The sum of their outputs is the turn input to one artificial axon. With this arrangement, if the light source in figure 9 was to the left of the car, the right photodiodes would output no turning voltage and the car would turn left toward the light source.

The voltage output of one photodiode depends on the angle of incidence of the light falling on it. For small angles θ (counted from normal incidence), the voltage drops as $\cos(\theta)$, and for larger angles the voltage drops sigmoidally to zero at $\theta\sim 60$ degrees. As an example, and referring to figure 9, with the light source in the NE direction, the forward and outward-facing photodiodes contribute input to the AA for right turns. The backward-facing photodiode is in the dark and therefore does not contribute to the AA input. For each eye, the ground pin of one photodiode is connected to the amplifier output of the next. The result is one output voltage from all three photodiodes, equal to the sum of their individual outputs. The summed output is con-

verted to a frequency and sent wirelessly to the corresponding artificial axon.

Although it is not necessary, for these navigation experiments we chose the photodiode circuitry such that even far away from the light source but at normal incidence, the photodiode output saturates. Specifically, we chose the transimpedance resistance so that the photodiode saturates at 5 m from the 625 nm, 100 W LED light source.

Source and terrain

Heating and background in the high-wattage LED are minimized with an active heat sink and brightness shields, respectively. Silicone thermal grease is applied to the interface between the LED and a heat sink for improved thermal conduction. Background refers to reflection of light from the floor and walls that adds a constant to the photodiode voltage output and is roughly independent of car orientation. The CLVC competes with this background and membrane leaks to keep the axon at the resting potential, and struggles when leaks alone are large. A brightness shield above the LED lowers background from reflection off the ceiling and walls, and a shield below the LED reduces background from floor reflection. Walls and reflective surfaces are covered with black tarps for background reduction. In total, shielding reduces the background to less than 5% of the photodiode saturation voltage.

Wireless communication

The Burr-Brown VFC32 converts the photodiode voltage output to a digital pulse input for the wireless transmitter. An external resistor value is chosen to make the VFC frequency linearly proportional to the photodiode output, and an external capacitor value is chosen to cap the frequency maximum at 4kHz. Two separate radio wave transmitters are used for left/right turning, 433 and 315 MHz, one transmitter for each direction. Encoder/decoder components typically paired to transmitters/receivers are excluded here because there is no interference between transmitters, and there is no interference from other devices in the

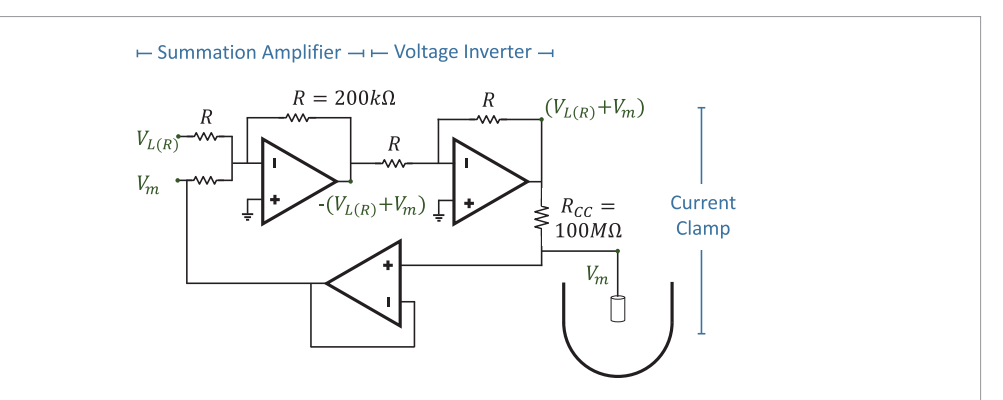


Figure 10. Schematic of the current clamp. The green dots represent the positions of the stated voltage values, also in green. The current clamp has three components: a summation amplifer circuit, a voltage inverter, and a high-impedance voltage follower. The potential difference between the voltage inverter and follower determines the current injected into the AA as $I_{CC} = V_{CC}/R_{CC}$.

lab where the navigation demonstration is performed. Furthermore, these simple receivers struggle with transmitted data frequencies above 17 kHz, but encoder oscillator frequencies must be larger than this to transmit VFC input in the kHz range.

Unlike voltage-to-frequency, the frequency-tovoltage conversion is done by software. While the VFC32 can convert frequency to voltage, the wireless receiver outputs a frequency duty cycle that is different from the VFC. To correct for the mismatch by hardware is unnecessarily complicated. Therefore, the frequency to voltage conversion is instead done by computer using LabVIEW. The program converts frequency to voltage, which is then fed to the input of the current clamp which forms the 'synapse' injecting into the AA. The command voltage to the clamp is thus $V_{cc} = \alpha f$ where f is the receiver frequency and α is a proportionality constant. There are two independent circuits for the right and left axons. The constant α is chosen so that it matches the electrophysiology characteristics of the corresponding axon (mainly dependent on leak current, Nernst potential, number of channels) and is therefore different between axons. For the run of the movie, we had $\alpha_L = 2.1 \,\mathrm{mV} \,\mathrm{kHz}^{-1}$ for the left axon and $\alpha_R = 1.8 \,\mathrm{mV} \,\mathrm{kHz}^{-1}$ for the right axon. The receiver output becomes noisy at frequencies near zero, so an added filter is written into LabVIEW to filter out this frequency noise. LabVIEW interprets this noise as large frequencies as high as 15 kHz. The filter removes frequencies higher than 3900 Hz, before the voltage conversion.

Current clamp

A schematic of the current clamp is shown in figure 10. All op-amps used are the low-noise FET precision op-amp AD795. The summation amplifier adds the command voltage V_{CC} to the membrane voltage V_m as $-(V_{CC}+V_m)$, and the inverter flips the voltage reference so that the sum is positive. The potential difference across the 100 M Ω current clamp resistor R_{CC} is V_{CC} , and the current injected is V_{CC}/R_{CC} . The high-impedance voltage follower measures V_m for feedback to the summation amplifier.

CLVC protocol

The CLVC protocol during firing (V_C , figure 2) is incidental to the particular inactivation dynamics of the KvAP. Channels will completely inactivate if the membrane potential is not pulled down to a large negative value after firing. The channel recovery rate from inactivation has a sigmoidal dependence on the membrane voltage, with the turning point at about -100 mV. Pulling the membrane voltage down to ~ -100 mV is typically sufficient to maintain firing.

For the run of the movie, the following settings were used. For the left axon: when the membrane voltage reaches the trigger value $V_T=4.5\,$ mV, the command voltage to the CLVC changes from $V_C(1)=-127\,$ mV to $V_C(2)=-455\,$ mV for $t_T=1.3\,$ s, pulling the membrane voltage to a large negative value. For the right axon: $V_T=0\,$ mV, $V_C(1)=-145\,$ mV, $V_C(2)=-364\,$ mV, $V_T=1.0\,$ s.

The clamp value $V_C(2)$ is chosen with a big safety margin to address the fact that sometimes the leak conductance of the AA changes in the course of a run. For example, you can see in figure 7(a), looking at the negative swings of the spikes, that the envelope of the spikes is roughly constant (at \sim -280 mV) for 0 < t < 80 s, then increases for 80 < t < 100 s, then stabilizes again (at \sim -120 mV) for t > 100 s. This increase is caused by an increase in leak conductance of the axon, from $\sim (83 \text{ G}\Omega)^{-1}$ to $\sim (2.4 \text{ G}\Omega)^{-1}$, approximately. However, even with the increased leak, the same CLVC protocol is able to pull the resting voltage down below -100 mV, allowing the channels to recover from inactivation and so be able to fire repeatedly. Similarly, you see that in the right axon (figure 7(b)) the leak conductance increases and then decreases again for 20 < t < 50 s. The origin of these slow fluctuations in leak conductance is presumably that the interface between lipid bilayer and solid support is not as stable as one would wish, in the present system. Similar fluctuations in leak conductance are observed even in the absence of channels, so this is a membrane phenomenon. In our present system, a membrane with channels lasts typically ∼10 min before it breaks; exceptionally we have lifetimes of \sim 1 h. Without channels, a membrane lasts typically 1 hr before the decane that suspends the lipids slowly falls by gravity onto the aperture, shrinking the membrane until the lipids are entirely re-suspended. Bursting aside, this one-hour timescale issue may be improved with a flat support structure geometry. The reason why with channels the membranes are even less stable is not clear. One guess is that the channels slowly cluster at the bilayer—support interface, leading to rupture. In any case, we will need to significantly improve the stability of the system if we want to scale it up even modestly.

Electrophysiology parameters

For the run of the movie, the axon parameters were set/measured as follows. Left axon: at maximum photodiode output, the current clamp injects $I_{CC}^{max} = 74$ pA into the axon; the number of open channels at peak voltage is approximately N = 380; the membrane capacitance is C = 190 pF. Right axon: $I_{CC}^{max} = 64$ pA, N = 720, and C = 185 pF.

The vehicle

From the manufacturer (GPTOYS), left/right movement on the model S911 car's remote is controlled by a 5 k Ω potentiometer configured as a voltage divider. In our system, we removed the potentiometer and connected the car remote to a National Instruments NI USB-6008 data acquisition device (DAQ). Analog turn signals are given to the car remote by LabVIEW through the DAQ, in place of the potentiometer. The negative terminal of the remote's battery is connected to the DAQ's ground channel, and turn voltages are supplied by the DAQ to the remote's 'signal' pin in the voltage divider circuit.

The smallest-radius left turn corresponds to a 0V signal with respect to ground. The smallest-radius right turn corresponds to 3V, and forward directed wheel orientation corresponds to 1.5V. Signal values between 0V and 3V correspond to larger turn radii that decrease linearly as the signal moves away from 1.5V in either direction. When an axon's membrane potential exceeds the set trigger voltage, LabVIEW sends an analog voltage signal to the car remote to make a smallest-radius turn in the direction of the axon that fired. The analog turn signal persists until LabVIEW detects a voltage signal (from the other axon) to turn in the opposite direction.

From the manufacturer, forward motion of the car is also controlled by a 5 k Ω potentiometer configured as a voltage divider in the car remote. The stop position corresponds to a 3 V signal, and maximum speed corresponds to a 0 V signal. In the remote's circuit protocols for forward motion, the applied signal must be at 3 V when the remote is turned on. The car begins to move at 150 mV below 3 V, i.e. 2.85 V. For compatibility with the slow (\sim 1 Hz) firing rate of our axons, we had to slow down the car. We introduced two modifications. First, a LabVIEW function generator supplies square

pulses with amplitude ~ 150 mV and period 500 ms for forward motion, with an offset chosen so that the maximum voltage is 3 V. Second, four 50 W resistors are connected in parallel to the car's motor to reduce the motor's current. This is a high current RC motor, so the power resistors are necessary. These modifications bring the car's speed down to 20-30 cm s⁻¹.

Discussion

Our goal with this demo is to instigate the development of 'ionic networks' [1]. We submit that a large network of artificial axons connected by tunable synapses would form an interesting neuroscience breadboard. One use would be to analyze principles of how the 'microscopics' of action potentials may give rise to macroscopic behavior. We note in passing that such a program is within the traditional focus of condensed matter physics, which seeks to understand 'emergent' macroscopic properties starting from the microscopic components and interactions. At a higher level of description, the relation between information flow and behavior need not be based on complicated rules in order to produce complex behavior. In his delightful book 'Vehicles', Valentino Braitenberg explains how simple control mechanisms can lead to surprisingly complex behavior [27]. His very first example in the book is the car with left/right control. However, the specific microscopics of action potentials puts constraints on the flow of information and also provides specific mechanisms for the interaction of different bits of information. If we believe that the latter process is essential for 'thought', we want our test network to be based on nodes which support action potentials. Even our simple, non-interacting system is not trivial to analyze, if one gets into a little detail, though it is easy enough to simulate.

Because of the difficulty of analytical work on the system, and because the experiment is very delicate at present, we created a simulation to explore the dynamical system properties. It is a simulation of the actual system: the artificial axon's dynamics are described with the Hodgkin-Huxley model, as in [1]; the eyes of the car receive light from the source depending on the orientation and distance of the car to the source; a proportional current is input into the corresponding Axon; the spikes in the Axon control the right—left turns, as in the experiments. The initial conditions and chosen parameters in the simulation resemble—but are not fit to—those of the experiment. In more detail, the simulation is performed as follows. For the dynamics of one artificial axon, we use the equation described in [1] for charging the membrane capacitance *C*:

$$C\frac{dV}{dt} = N_0(p_O \chi + \chi_\ell)[V_N - V(t)] + \frac{1}{R_C}[V_{CLVC} - V(t)] + \frac{1}{R_{CC}}V_{CC}(t).$$
 (2)

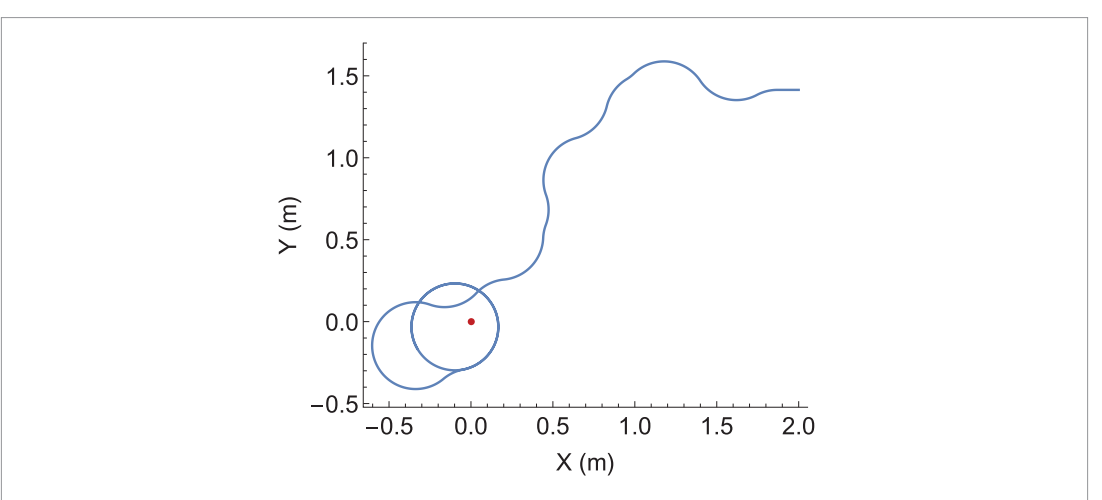


Figure 11. Car trajectory obtained from a simulation where the right AA has a firing rate 1.9 times higher than the left AA, for the same light seen. The car still 'finds' the light source, which is at the origin.

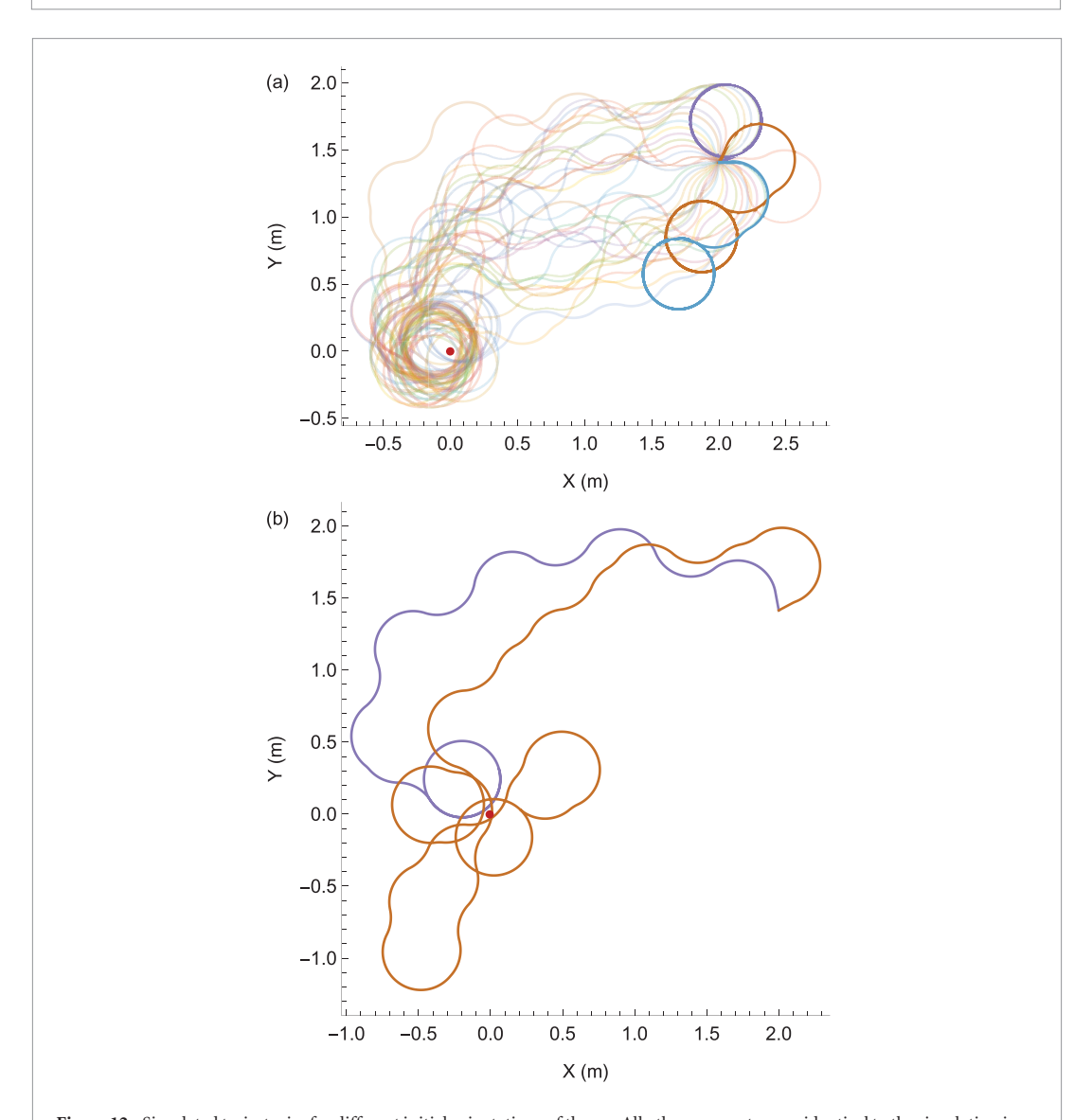


Figure 12. Simulated trajectories for different initial orientations of the car. All other parameters are identical to the simulation in figure 11. The transparent traces in (a) represent trajectories that end in a successful navigation limit cycle, and the bold traces are three examples of navigation failures. The trajectories in (b) are interesting cases; the purple trajectory is a navigation failure, and the brown trajectory is a success that requires multiple approaches to the source to reach a successful-navigation limit cycle.

Here, N_0 is the number of channels, χ and χ_ℓ are the open channel and leak conductances, V_{CIVC} and R_C are the current limited voltage clamp set voltage and load resistance, and V_{CC}/R_{CC} is the current injected by the current clamp. The term $p_O = p_O(V,t)$ is the voltage-dependent channel open probability. It is part of a set of rate equations for the channel behavior, which are combined with equation (2) as a system of differential equations. These rate equations and rate constants are described in [1, 22], and together with (2) form the Hodgkin–Huxley model. The current clamp voltage V_{CC} is proportional to V_p , the sum of the photodiode output:

$$V_{CC} = c \sum_{i=1}^{3} V_{p}^{(j)}(\theta_{j}, s).$$
 (3)

The variable c is a scaling constant that puts V_{CC}/R_{CC} in the picoAmp range. θ_j is the angle of incidence on the jth photodiode, and s is the distance between the light source and the eye in figure 9; s is approximated to be some point at the center of the three photodiodes. The photodiode output $V_p(\theta_j, s)$ is fit to the behavior of the OPT301.

The position of the car in time is represented by a vector $\mathbf{L}=(x,y)$. The turning motion of the car is treated as uniform circular motion, with acceleration $\mathbf{a}=\boldsymbol{\omega}\times\mathbf{v}$ and $\boldsymbol{\omega}=(k\hat{\mathbf{z}})v/r$, where r is the turn radius of the car. Left–right turning is a change in the direction of the angular frequency by the index k. The turning protocol is as follows: when the right axon R spikes, k is set to +1 and remains fixed; when L spikes, k switches to -1. The equations of motion for the car are:

$$\ddot{x} = k(t) \frac{v}{r} \dot{y}$$

$$\ddot{y} = -k(t) \frac{v}{r} \dot{x}.$$
(4)

The orientation of the car is given by the velocity vector. The complete model consists of a system of equations, composed of equation (4) and two sets of the following, one for each Axon: the membrane equations (2), (3) and the rate equations for p_O described in [1]. We set initial conditions x(0), y(0), $\dot{x}(0)$, $\dot{y}(0)$, with $k(0) \approx 0$, and solve numerically.

Sources of noise are not included in the simulation, which is in that way deterministic. In the experiments, there are on the contrary sources of randomness at all scales, from the tires of the car slipping on the oor, resulting in a non steady speed, to the stochastic nature of the ion channels dynamics.

Let us come back to the issue of different firing rates for equal light intensity. Figure 11 shows the trajectory from a simulation with similar initial conditions as the movie (see materials and methods for details). In the simulation, the right AA had a firing rate 1.9 times higher than the left AA, for the same light received at the photodiode. The right turn bias is visible in the car's trajectory, but overall the car still finds the light

source. The end state is a limit cycle which is a circle containing the light source. On the limit cycle of this successful navigation trial, one eye faces away from the light source at all points on the circle trajectory, and the input to this outward-facing axon is ~ 0 .

How much difference in the firing rates can be tolerated depends on the other parameters of the system. For example, with the firing rate ν , the car speed u, the turn radius of the car r, the initial distance to the light source L, we can form the two dimensionless numbers $\chi = u/(\nu r)$ and $\rho = r/L$. Then we can discuss, in this parameter space, the basin of attraction of the set of limit cycles which form the desirable end states. However, this is already a complicated question to explore analytically, for such a simple dynamical system!

A study of the phase diagram of the system is beyond our present scope, but in order to start to address questions of stability and robustness we have performed a series of simulations for varying initial conditions. As a first step, we varied only the initial orientation of the car with respect to the light source, keeping all other parameters fixed. The results are as follows.

- The system appears stable in that the same initial condition results in the same trajectory.
- Given the starting point of figure 11, for (2) $25^{\circ} < \varphi < 360^{\circ}$, where φ is the initial direction of the car counted counterclockwise from East, the system converges to the desired limit cycle containing the light source. For $0^{\circ} < \varphi < 25^{\circ}$ the system generally gets stuck in a different limit cycle. In figure 12(a) the bold, blue trace corresponds to the initial angle $\varphi = 0^{\circ}$. The transparent traces all end in successful navigation limit cycles, and the bold traces are a few of the navigation failures. In these failures, both axons are still firing. However, the channels are in a state of high inactivation, so the spikes' amplitudes are insufficient to reach the trigger voltage that changes k for turning. This is the behavior with parameters chosen to mirror those in the experiment, however, these navigation failures can be removed in the simulation by raising the Nernst potential sufficiently to bring all spikes to the trigger voltage.
- (3) Within the basin of the successful trajectories, there are certain values of φ which lead to much longer trajectories, with multiple approaches to the source before the desired limit cycle is found. Figure 12(b) presents such a case. The purple trace is a failure that is corrected by increasing the Nernst potential, like the traces in figure 12(a). The brown trace is a result of the phase phenomena and right-turn bias described for the experiment. As

the vehicle in the simulation approaches the light source, the phase of the action potentials conspires to move the vehicle away from the origin. The vehicle continues to return to the source until its trajectory indefinitely positions one eye away from the source. In short, for these trajectories the car quickly 'finds' the source, but takes multiple approaches to find the limit cycle.

Looking to the future, we are far from being able to construct a self-contained ionic network. Some of the difficulties seem surmountable with present day engineering, others would require new inventions. In the context of this demo, for example, we can see a path for substituting some of the electronic components with ionics. The CLVC could be dispensed with by adding a second ionic gradient, e.g. of Na⁺, and corresponding voltage gated ion channels. Photodiodes could in principle be replaced by AAs with embedded channel rhodopsin. On the other hand, ionics based 'synapses' compatible with the 100 mV scale of ionic action potentials require new inventions. Finally, 3D printing technology currently being developed to produce scaffolds for directed neuronal growth [28] could probably form the basis for scaling up our AA network.

Acknowledgments

This work was supported by funds from the Dean of Physical Sciences at UCLA, and by NSF grant DMR 1809381. We thank Albert Libchaber for pointing us to Valentino Breitenberg's book.

ORCIDiDs

Hector G Vasquez https://orcid.org/0000-0003-2009-5871

References

- [1] Vasquez H G and Zocchi G 2017 Coincidences with the artificial axon *Europhys. Lett.* **119** 48003
- [2] Ariyaratne A and Zocchi G 2016 Toward a minimal artificial axon J. Phys. Chem. B 120 6255
- [3] Ananthanarayanan R, Esser S K, Simon H D and Modha D S 2009 The cat is out of the bag: cortical simulations with 10⁹ neurons, 10¹³ synapses Proc. of 2009 IEEE/ACM Conf. on High Performance Computing Networking, Storage and Analysis
- [4] Indiveri G et al 2011 Neuromorphic silicon neuron circuits Frontiers Neurosci. 5 73
- [5] Pfeil T et al 2013 Six networks on a universal neuromorphic computing substrate Frontiers Neurosci. 7 11
- [6] Wyart C et al 2002 Constrained synaptic connectivity in functional mammalian neuronal networks grown on patterned surfaces J. Neurosci. Methods 117 123

- [7] Feinerman O, Segal M and Moses E 2005 Signal propagation along unidimensional neuronal networks J. Neurophysiol. 94 3406
- [8] Feinerman O and Moses E 2006 Transport of information along unidimensional layered networks of dissociated hippocampal neurons and implications for rate coding J. Neurosci. 26 4526
- [9] Chang J C, Brewer G J and Wheeler B C 2006 Neuronal network structuring induces greater neuronal activity through enhanced astroglial development J. Neural Eng. 3 217
- [10] Feinerman O, Rotem A and Moses E 2008 Reliable neuronal logic devices from patterned hippocampal cultures *Nat. Phys.* 4 967–73
- [11] Marconi E et al 2012 Emergent functional properties of neuronal networks with controlled topology PLoS One 7 e 34648
- [12] Pasca A M et al 2015 Functional cortical neurons and astrocytes from human pluripotent stem cells in 3d culture Nat. Methods 12 671
- [13] Schuman C D et al 2017 Survey of neuromorphic computing and neural networks in hardware (arXiv:1705.06963)
- [14] Potter S M, Wagenaar D A, Madhavan R and DeMarse T B 2003 Long-term bidirectional neuron interfaces for robotic control, and in vitro learning studies Proc. of the 25th Annual Int. Conf. of the IEEE Engineering in Medicine and Biology Society (IEEE Cat. No.03CH37439) vol 4 pp 3690–3
- [15] Shahaf G, Eytan D, Gal A, Kermany E, Lyakhov V, Zrenner C and Marom S 2008 Order-based representation in random networks of cortical neurons PLoS Comput. Biol. 41–11
- [16] DeMarse T B and Dockendorf K P 2005 Adaptive flight control with living neuronal networks on microelectrode arrays *Proc.* IEEE Int. Joint Conf. on Neural Networks vol 3 pp 1548–51
- [17] Schneider M L et al 2018 Ultralow power artificial synapses using nanotextured magnetic josephson junctions Sci. Adv. 4 4526
- [18] Ariyaratne A and Zocchi G 2013 Nonlinearity of a voltage gated potassium channel revealed by the mechanical susceptibility Phys. Rev. X 3 011010
- [19] Heginbotham L, Kolmakova-Partensky L and Miller C 1998 Functional reconstitution of a prokaryotic k^+ channel *J. Gen. Physiol.* 111 741–9
- [20] Rigaud J-L, Levy D, Mosser G and Lambert O 1998 Detergent removal by non-polar polystyrene beads Eur. Biophys. J. 27 305–19
- [21] Aimon S, Manzi J, Schmidt D, Poveda Larrosa J A, Bassereau P and Toombes Gilman E S 2011 Functional reconstitution of a voltage-gated potassium channel in giant unilamellar vesicles PLoS One 6 e25529
- [22] Schmidt D, Cross S R and Mackinnon R 2009 A gating model for the archeal voltage-dependent k⁺ channel KvAP in DPhPC and POPE:POPG decane lipid bilayers J. Mol. Biol. 390 902–12
- [23] Ruta V, Jiang Y, Lee A, Chen J and MacKinnon R 2003 Functional analysis of an archaebacterial voltage-dependent K+ channel Nature 422 180-5
- [24] Jiang Y, Ruta V, Chen J, Lee A and MacKinnon R 2003 The principle of gating charge movement in a voltage-dependent k^+ channel Nature~423~42-8
- [25] Jiang Y, Lee A, Chen J, Ruta V, Cadene M, Chait B T and MacKinnon R 2003 X-ray structure of a voltage-dependent K⁺ channel Nature 423 33–41
- [26] Wang A and Zocchi G 2011 Artificial modulation of the gating behavior of a k^+ channel in a kvap-dna chimera *PLoS One* 6 1–8
- [27] Braitenberg V 1984 Vehicles (Cambridge, MA: MIT Press)
- [28] Espinosa-Hoyos D et al 2018 Engineered 3D-printed artificial axons Sci. Rep. 8 478